

Abram R. Jacobson*

Los Alamos National Laboratory, Los Alamos, New Mexico

1. INTRODUCTION

Space-based monitoring and mapping of lightning has recently enjoyed substantial progress due to two extremely successful optical imagers, the Optical Transient Detector, or OTD [Boccippio, D. J. et al., 2000], and the Lightning Imaging Sensor, or LIS [Christian, H. J. et al., 1999]. Progress has also been made on defining the utility of broader types of lightning observations in general, as a proxy for deep tropospheric convection [Boccippio, D. J. et al., 2000; Petersen, W. A. and Rutledge, S. A., 1998; Zipser, E. J., 1994; Zipser, E. J. and Lutz, K. R., 1994], as a real-time indicator of imminent severe weather [Williams, E. R., 2001; Williams, E. R. et al., 1989], and as a data constraint on meteorological simulations [Chang, D.-E. et al., 2001].

Compared to optical imagery, reception of radio-frequency (RF) emissions from lightning processes offers a somewhat less direct, but complementary means of remotely sensing lightning from space [Holden, D. N. et al., 1995; Jacobson, A. R. et al., 1999; Jacobson, A. R. et al., 2000; Massey, R. S. and Holden, D. N., 1995; Massey, R. S. et al., 1998]. This remote-sensing capability might eventually allow existing RF receivers on satellite constellations to perform real-time tracking of the deep tropospheric convection with which lightning is associated in certain well-characterized and important weather regimes [Boccippio, D. J. et al., 2000; Petersen, W. A. and Rutledge, S. A., 1998; Zipser, E. J., 1994; Zipser, E. J. and Lutz, K. R., 1994]. The location of the lightning could be determined via RF measurements simultaneously from a constellation of sensors performing time-difference-of-arrival (TDOA) signal processing.

Potential benefits of this approach include retrieval of the height of the lightning emission, which is an indicator of the vigor of the convective system and which is thought to be a predictor of the likelihood of severe weather [Williams, E. R., 2001]. Another potential benefit of RF lightning records is identification, from the RF waveform, of the specific lightning process, e.g. return stroke, intracloud leader, etc. At present we do not adequately understand how to infer convective-storm characteristics from radio-frequency signals collected in space. Reaching such an understanding requires detailed and systematic study of large collections of RF signals recorded under the observational constraints of a space-borne sensor. This can be done with single research satellites, albeit without the location capabilities of constellation TDOA. In the following, we present preliminary observations on the meteorological context of the intense RF pulses. Since the use of lightning RF emissions as a proxy for severe convection monitoring from space is a new idea, it is necessary to demonstrate a close connection between the incidence of RF pulses and meteorologically significant convective structures. If the connection is either not close, or not reliable, then the RF pulses would be of questionable remote-sensing value.

2. PULSE CHARACTERISTICS

Figure 1 shows the appearance of the two intracloud-lightning radio pulses most frequently seen by the FORTE satellite [Jacobson, A. R., 2003; Jacobson, A. R., 2003; Jacobson, A. R. and Light, T. E. L., 2003; Jacobson, A. R. et al., 1999]. The top pulse shown is the strong radio emission that is most useful for remote sensing applications, due to its ability to be detected by radio receivers at GPS altitudes, where a deployed system will be located [Suszcynsky, D. et al., 2000; Suszcynsky, D. M. and Heavner, M. J., 2003].

* *Corresponding author address:* Abram R. Jacobson, LANL, Mail Stop D436, Los Alamos, NM 87545; e-mail: ajacobson@lanl.gov

The strong radio pulses are observed to occur frequently in severe thunderstorms, though

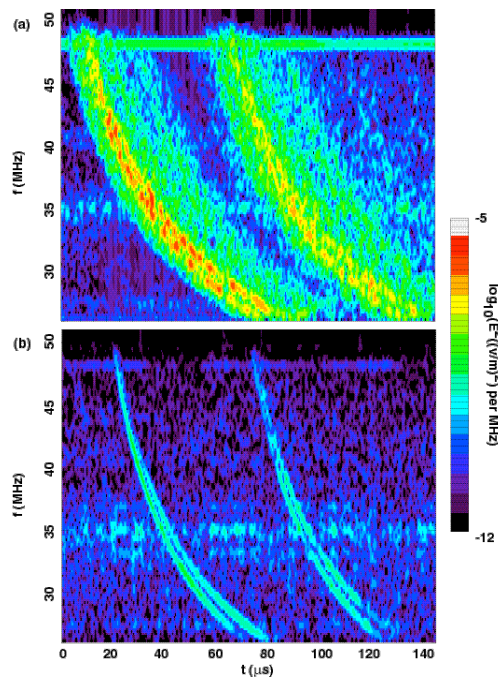


Figure 1: Spectrograms of (a) strong intracloud pulse, and (b) weak polarized/coherent intracloud pulse. The ground echo is at a delay of $\sim 50 \mu\text{s}$ relative to the main pulse.

presently our knowledge of their incidence is based mainly on data from FORTE and is therefore only preliminary. The remainder of this article presents the evidence to date addressing whether the strong radio pulses are a viable remote-sensing proxy for severe convection.

3. RELATION OF STRONG RADIO PULSES TO NARROW BIPOLAR EVENTS

The strong radio pulses seen in the VHF spectrum by FORTE and by the ground-based Lightning Mapping Array (LMA) [Rison, W. et al., 1999; Thomas, R. J. et al., 2001; Thomas, R. J. et al., 2000] appear to be precursors of the “Narrow Bipolar Event” (NBE), an intracloud large-scale current flow that is finished within a short time ($10 \mu\text{s}$) relative to normal leader processes [Smith, D. A. et al., 2004; Smith, D. A. et al., 2002; Smith, D. A. et al., 1999]. Figure 2 shows the appearance of

both polarities of NBE, as well as a conventional lightning discharge, as seen on low-frequency (LF; 30-300 kHz) vertical-electric-field recorders.

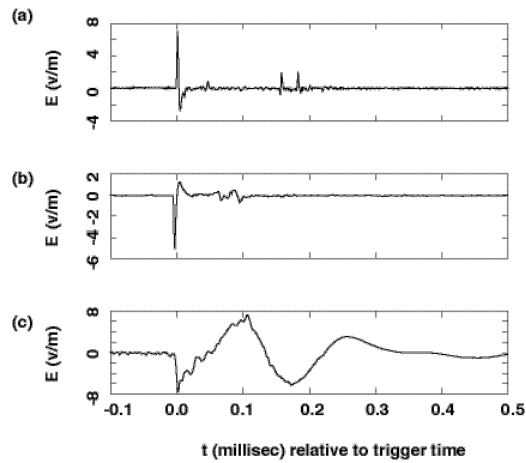


Figure 2: Los Alamos Sferic Waveform Array vertical electric field data examples for (a) a Narrow Positive Bipolar Event (NPBE), (b) a Narrow Negative Bipolar Event (NNBE), and (c) an ordinary sferic.

The strong VHF emissions (Figure 1 a) are occasionally accompanied by an NBE (Figure 2 a,b). However, an NBE is *always* accompanied (at least in observations to date) by a strong VHF emission.

4. METEOROLOGICAL SETTING OF NARROW BIPOLAR EVENTS: COMPARISON WITH ORDINARY LIGHTNING

We have used the Los Alamos Sferic-waveform Array (LASA) [Smith, D. A. et al., 2002] centered on the Florida region to study the incidence of both ordinary and NBE lightning discharges in characterized meteorological settings. LASA is a research tool developed by the Los Alamos National Laboratory (LANL) for ground support of the FORTE satellite and of the VHF radio sensors on the GPS satellites. The electric-field waveform is sampled at a rate of 1 megasample/s (so that the Nyquist bandpass is 0.5 MHz). Typically 8192 samples (8.192 millisecond) of data are contained in a record for a single trigger. The LASA system returns full waveform records to the network headquarters (in Los Alamos, New Mexico) daily for analysis

and attempted identification of the causative lightning process. The choices of lightning process include +NBE, -NBE, +CG, -CG, and “undetermined”. The automated algorithm for identification of LASA-recorded waveforms is conservative; most of the “undetermined” events that are checked by eye appear to be probable ground strokes. For either polarity of NBE, the discharge height can often be determined [Smith, D. A. et al., 2004]. Both of these features –return of the full waveform, and retrieval of the emission height for some NBE discharges –are unique to LASA and not currently available in operational lightning-location systems based on signals in the low-frequency (30-300 kHz) and very-low-frequency (3-30 kHz) range. This ability to archive and to examine full waveforms is the reason for the LASA research facility. We can identify the various types of lightning discharges based on detailed examination of the waveform. Summing over the various types of identifications, there were 3,073,907 acceptable, located LASA lightning events during the 1999-2002 period.

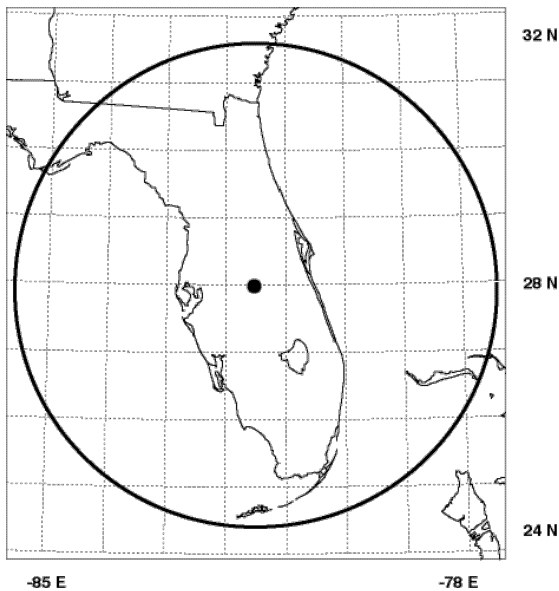


Figure 3: Map of Florida study area, with 400-km-radius circle centered on -81.5 E, 28.0 N. The lightning-location grid extends over 8 deg X 8 deg centered on this point, with 0.2 -deg X 0.2 -deg pixels.

The study area is a circle of 400-km radius centered on -81.5 deg E, 28 deg N.

In order to compare the behavior of NBEs and the more conventional cloud-to-ground discharges (CGs), we have divided the 8 -deg X 8 -deg study zone (see Figure 3) into 40 X 40 pixels (1600 pixels total), each pixel measuring 0.2 -deg X 0.2 deg, or ~ 20 -km (E-W) X 22 -km (N-S). This is within a factor-of-two of the typical convective-cell size (~ 10 km) in either air-mass thunderstorms or multicellular fronts. We have divided time into windows of duration 10 minutes (600 s), advanced by half a window width (5 minutes, or 300 s). Thus each three-dimensional spatio-temporal data pixel is spaced by 20 -km (E-W) X 22 -km (N-S) X 300 s.

The first step in testing the spatial relationship between NBEs and ordinary lightning is to estimate the covariances versus spatial and temporal separation. We use an 11 -pixel X 11 -pixel sliding window centered on the pixel containing the key event. We look for neighbors of the key event in all 121 pixels in the 11 -pixel X 11 -pixel sliding window, and we take the product of the central-pixel population of key events times the populations of all 121 pixels in the sliding window. This gives 121 products, representing discrete sampling of different separations. We then sum that product matrix over all 300-sec time steps and over all days in the four-year period 1999-2002. Finally, we re-order the 121-element matrix elements by isotropic distance from the key event.

Based on the summed population-product matrix, we calculate the normalized correlation versus isotropic separation. Because Florida (see Figure 3) is not isotropic but rather is a peninsula, and tends to impose some degree of N-S elongation on the storm activity, the spatial correlation shows slight departures from isotropy.

Figure 4 shows three correlation functions, truncated to highlight the correlation range 0.0 to 0.4. The heavy solid curve is the autocorrelation of $-CG$ populations, normalized to unity at zero separation. The light solid curve is the autocorrelation of $+NBE$ populations, also normalized to unity at zero separation. The heavy dashed curve is the

cross-correlation of $-CG$ populations with $+NBE$ populations. The cross-correlation's zero-separation value is only 29%, but the heavy dashed curve has been artificially amplified by $1/0.29$ to allow ready comparison with the two autocorrelation functions.

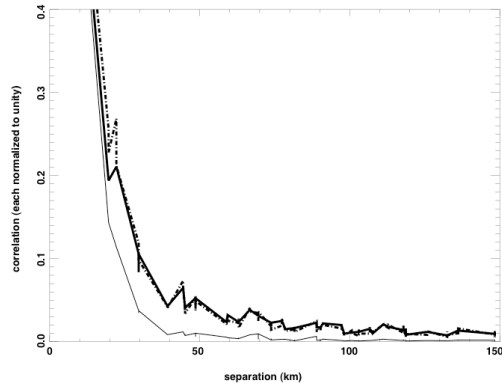


Figure 4: Equal-time, spatial correlation functions versus isotropic separation. All curves are truncated at 0.4 even though their highest point (at zero separation) is unity. Heavy solid curve: Autocorrelation function of $-CG$ pixel occupancy. Light solid curve: Autocorrelation function of $+NBE$ pixel occupancy. Heavy dashed curve: Cross-correlation function of $-CG$ with $+NBE$ pixel occupancies, multiplied by factor $1/0.29$ to compensate for 29% correlation at zero separation. The fine-scale irregularities are caused by anisotropies (see text).

The fine-scale irregularities in all three curves in Figure 4 are due to the slight anisotropies in the correlation matrix. Despite this anisotropy, all three correlations fall off clearly with increasing isotropic separation. The $-CG$ autocorrelation (heavy solid curve) is wider than the $+NBE$ autocorrelation (light solid curve), below the 0.2 correlation level. The cross correlation mimics the wider autocorrelation. These relationships indicate that NBEs tend to occur in spatially tighter sub-zones of the storms compared to ordinary lightning. The 29% cross-correlation of $+NBE$ s with $-CG$ s in Florida is highly significant, as the statistical noise (tail value at right end of heavy dashed curve) is only < 0.02 .

The results in Figure 4 have shown the equal-time correlations as a function of spatial separation. Now we reverse the procedure and examine the zero-separation correlations as a function of temporal separation δt . Figure 5 shows the temporal autocorrelations for (a) $-CG$ s, (b) $+NBE$ s, and (c) $-NBE$ s. In each panel, the solid curve is without any spatial smoothing, while the dashed curve is with 5-pixel X 5-pixel (approximately 100-km) spatial smoothing.

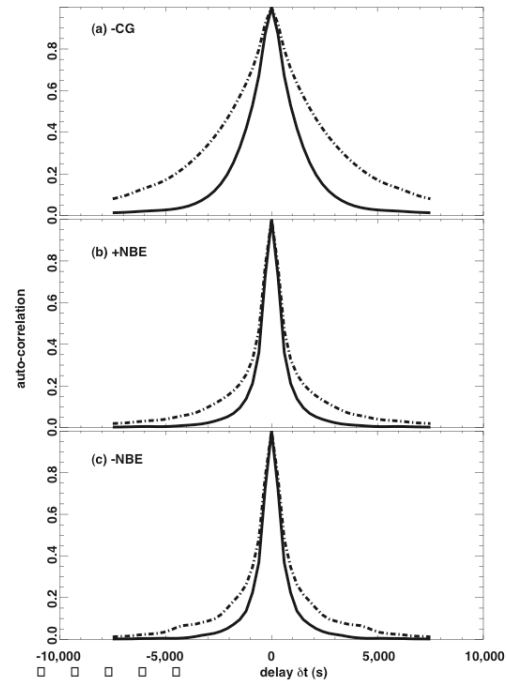


Figure 5: Zero-separation, temporal autocorrelation functions for (a) $-CG$ pixel occupancies, (b) $+NBE$ pixel occupancies, and (c) $-NBE$ pixel occupancies. Solid curves: Without further spatial averaging. Dashed curves: With prior spatial smoothing by 5-pixels X 5-pixels ($\sim 100\text{-km} \times 100\text{-km}$).

The halfwidth to $1/e$ for $-CG$ s is about 2500 s without spatial 100-km smoothing, and about twice that with spatial 100-km smoothing. The halfwidth to $1/e$ for each type of NBE is about 1200 s without spatial 100-km smoothing, and only about 25% more with spatial 100-km smoothing.

Two features are apparent: First, the duration of NBE occurrences during a given storm tends to be only half the duration of $-CG$

occurrences in the same storm. Second, the distribution of $-CGs$ is two-fold wider in time if we first average over 100 km spatially, whereas the distribution of NBEs undergoes 25% further widening in time. This indicates that $-CGs$ appear in more phases of a developing/adverting storm complex than do NBEs (of either polarity.)

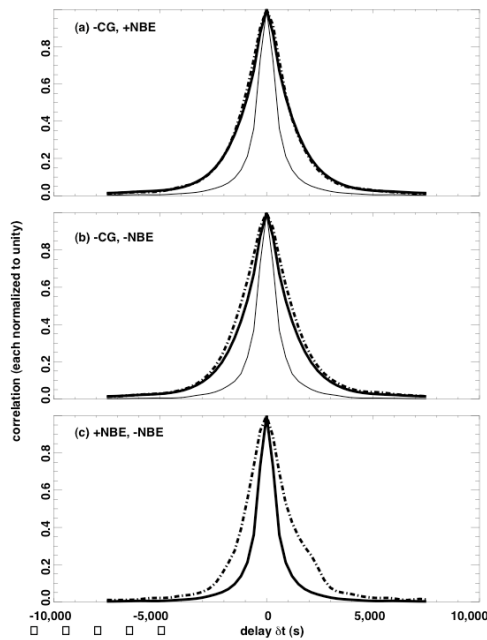


Figure 6: In each panel, two autocorrelation functions repeated from Figure 5 (heavy and light solid curves) and one cross-correlation function (heavy dashed curve), for (a) $-CGs$ and lagged $+NBEs$ (multiplied by factor $1/0.29$), (b) $-CGs$ with lagged $-NBEs$ (multiplied by factor of $1/0.16$), and (c) $+NBEs$ with lagged $-NBEs$ (multiplied by factor of $1/0.11$). The light solid curve in (c) is almost identical to, and therefore covered by, the heavy solid curve.

Lagged (as a function of lag δt) correlations can also address whether one type of lightning event tends to precede, or follow, another type during the development of storms. Figure 6 shows (heavy dashed curve) the correlation of (a) $-CG(t)$ with $+NBE(t+\delta t)$, (b) $-CG(t)$ with $-NBE(t+\delta t)$, and (c) $+NBE(t)$ with $-NBE(t+\delta t)$. In each panel the heavy solid curve is the first type's auto-correlation, the light solid curve is the second type's auto-correlation, and the heavy dashed curve is the cross-correlation. The latter is artificially multiplied by the inverse

of the cross-correlation coefficient to allow ready comparison to the auto-correlation functions. The autocorrelations in Figure 6 are the same as the auto-correlations in Figure 5 and are repeated to provide a comparison to the cross-correlations.

Figure 6 indicates that there is no systematic lag of NBEs (of either polarity) with respect to $-CGs$. Although NBEs (of either polarity) occur during a smaller duration of the storm lifecycle than do $-CGs$, the NBE occurrences are not systematically advanced or retarded with respect to the temporal centroid of $-CGs$. Similarly, to the small extent that $-NBEs$ coexist with $+NBEs$ (correlation: 11%), they have no systematic lag relationship (Figure 6c).

5. METEOROLOGICAL SETTING OF NARROW BIPOLAR EVENTS: COMPARISON WITH CLOUD-TOP TEMPERATURE

The purpose of this section is to determine whether NBEs behave as do $-CGs$ with respect to their spatial relationship to clouds. Ordinary lightning is far more likely to be accompanied by high (i.e., cold) cloud tops than to be accompanied by low (i.e. relatively warm) cloud tops [Williams, E. R., 2001]. Do NBEs behave similarly? We answer this with infrared cloud maps. These cloud maps at 10.7 microns (GOES East, IR channel #4) reveal the cloud-top temperature. The cloud-top temperature then serves as a crude cloud-top altimeter, assuming that the inferred temperature is in equilibrium with the environmental thermocline. This altimetry can be performed only in the monotonic portion of the thermocline, from ground to the tropopause. It is not expected that thunderclouds will occur in equilibrium above the tropopause, although a few km of overshoot can occur transiently for exceptionally vigorous convection [Williams, E. R., 2001]. At any rate, for cloud parcels that are in vertical motion and hence not in equilibrium with their surroundings, the altitude estimate from cloud-top temperature is erroneous.

The thermocline varies both diurnally and seasonally. Figure 7 shows temperature versus height from all radiosondes launched out of Cape Kennedy, Florida during 2001, regardless of local time and season. The radiosonde observations are provided by the Forecast Systems Laboratory of NOAA (<http://raob.fsl.noaa.gov>). Each of the 44,733 dots in Figure 7 is a reported temperature. The dots follow a well-defined and reproducible thermocline. Some anomalous outliers are obvious; all 2001 data are included without editing, including points with obvious errors. Superimposed on the data are isotherms (horizontal lines) from -20 deg C to -80 deg C, in steps of 10 deg C. Each isotherm's intersection with the observed thermocline is marked by a dashed vertical line at constant altitude. It is seen that the temperature tropopause occurs around ~ 15 -km altitude and at a temperature around -70 deg C. Thus it would not be expected to see thunderclouds above 15 km in equilibrium with their environment.

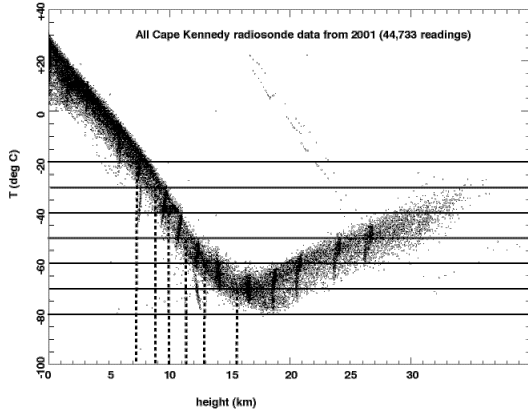


Figure 7: Cape Kennedy radiosonde temperature measurements versus height for all soundings during 2001. Spurious artifacts are included. Data from NOAA/Forecast Systems Laboratory (see text).

The first question is, do the NBEs occur at heights that are consistent with their being in the troposphere? If not, it would be difficult to associate them with thunderstorm phenomena. The NBE waveform often permits the automated retrieval of emission height [Smith, D. A. et al., 2004]. This was possible in about 2/3 of the NBEs used in this analysis with IR-imagery support. Figure 8 shows the distribution of inferred NBE emission height

based on automated processing of the waveform. The distribution peaks at 13-14 km altitude. Over 80% of the NBEs are emitted below 15 km. However, the $<20\%$ of NBEs in this distribution that are emitted in the range 15-20 km altitude are unlikely to be completely explainable as measurement artifacts. We believe our altitude-measurement uncertainties are <2 km, so it is likely that at least some of these events are truly occurring above the nominal tropopause. It remains unclear whether these high-altitude NBEs occur in clear air above the cloud tops (as in "blue jets" [Wescott, E. M. et al., 1998]) or occur in overshooting clouds that transiently exceed the equilibrium tropopause height.

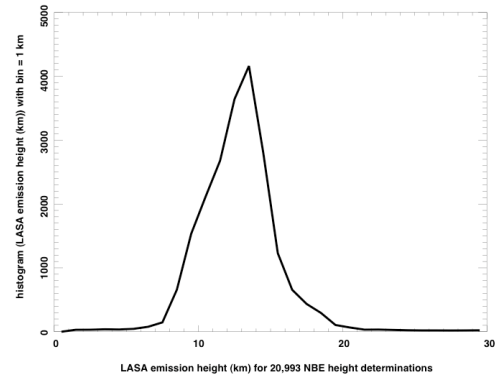


Figure 8: Distribution of NBE emission height for 20,993 NBE waveforms that allowed automated retrieval of ionospheric and emission heights (see text).

Fifteen-minute data on cloud-top-temperature were obtained from infrared (IR) channel 4 on NOAA's GOES-East satellite, via the NASA GSFC. A threshold was set to exclude entire days having <10 LASA events within the 400-km-radius circle, even if the GOES-East data was in our archive. The IR data was considered useable for a given lightning discharge only if the IR image was recorded within ± 15 minutes (900 s) of the lightning event's occurrence. Subject to these restrictions, the total number of accepted, IR-supported LASA events within the 400-km-radius circle was 1,054,836 during the period 1999-2002. This is about a third of the total number of lightning locations characterized by LASA within the 400-km-radius circle during that period.

Having determined that the NBEs tend to occur in the upper troposphere, we now examine what their relationship is with cloud heights as inferred from the cloud-top temperature. For this purpose, we do not use the lightning-event pixellation, but instead use the exact observed location of each lightning event. We use the pixels of the GOES-East image (which do *not* coincide with our 0.2-deg X 0.2-deg lightning pixellation) and compute the inferred cloud-top temperature for those pixels. For each lightning event detected by LASA, we gather all the image pixels whose centers lie within both 30-km, and 100-km, - radius circles centered on the lightning location. We then build two statistics from the cloud-top temperatures within each of these circles: First, we tally the full distribution of cloud-top temperatures within the circle centered on the lightning-event location.

Second, we tally the coldest cloud-top temperature within the circle. These two statistics are then accumulated over the entirety of LASA-located lightning events for which there is GOES-East imagery.

Figure 9 shows histograms of the distribution of cloud-top temperatures proximal to lightning, summed over all the IR images in the archive. The light solid curve is for the background distribution over all pixels in the entire scene, regardless of proximity to lightning locations. The heavy solid curve is for those pixels with a 30-km-radius circle proximal to each lightning event. The heavy dashed curve is for those pixels within a 100-km-radius circle proximal to each lightning event. The lightning events in Figure 9(a) are non-NBEs (+CG & -CG & undetermined), while those in Figure 9(b) are the NBEs (of both polarities summed together).

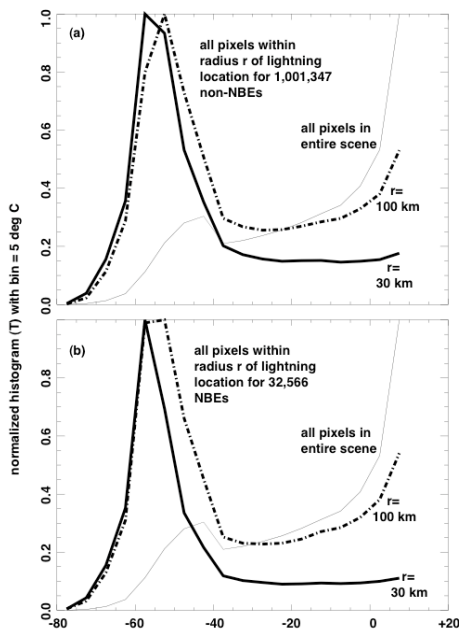


Figure 9: Distribution of cloud-top temperatures inferred from GOES-East IR (10.7-mm) imagery during times in 1999-2002 in which there was LASA data. Light solid curve: Background cloud distribution over entire Florida-area sub-image (see Figure 2). Heavy solid curve: Cloud distribution within 30-km proximity to each lightning event. Heavy dashed curve: Cloud distribution within 100-km proximity to each lightning event. (a) For non-NBE lightning. (b) For NBE lightning (both polarities).

First consider the background temperature distribution (light solid line) in both panels of Figure 9. Obviously it is the same curve in both Figures 9(a) and 9(b), because it is not conditioned by proximity to lightning. The steeply rising feature at the far right (high temperature) is the transition to clear skies. The smaller hump at -40 deg C to -50 deg C is the cloud signature. This cloud signature has a tail going out to -70 deg C, roughly as we would expect (see the radiosonde data in Figure 7) for deep convection.

Next, consider the distribution of cloud-top temperatures in proximity to either non-NBEs (Figure 9a) or NBEs (Figure 9b). The peak for either 30-km or 100-km proximity is located on the cold (left) tail of the background distribution, near -50 deg C to -60 deg C. According to the radiosonde thermocline (Figure 7), that corresponds to altitudes around 12 km. That is within the peak of the NBE altitude distribution inferred from the waveform data (Figure 8), so the two independent ways of constraining cloud height seem not to be radically inconsistent. For both non-NBEs (Figure 9a) and NBEs (Figure 9b), the distributions for $r=30$ km are colder than those for $r=100$ km. This is reasonable, in that the further away from the lightning location one allows the cloud pixel to be accumulated

in the statistic, the more chance of including shallower (lower) clouds that are near, but not immediately associated with, the lightning. This also explains the higher “bridge” value for $r=100$ km in the transition region (-40 deg C to 0 deg C). Further from the lightning, there is more low cloud, broken cloud, or even clear sky.

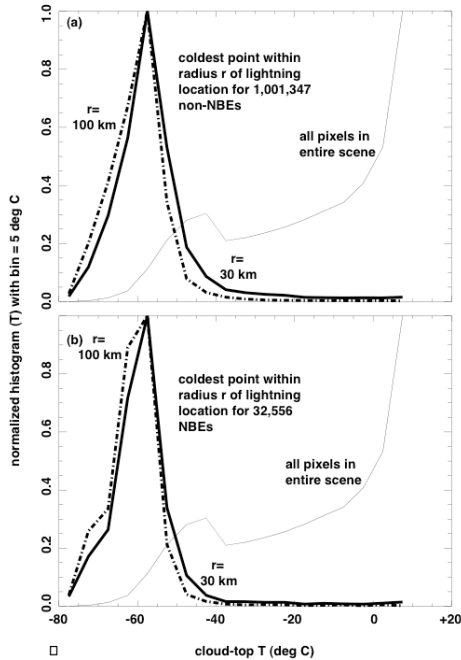


Figure 10: Light solid curve is identical to that in Figure 9, but heavy curves are distributions of *minimum* cloud-top temperature proximal to lightning events, within $r=30$ km (heavy solid curve) and within $r=100$ km (heavy dashed curve). (a) Lightning = non-NBEs; (b) lightning = NBEs.

Given that lightning can occur in compact updraft cells whose transverse size (<10 km) is not well resolved in GOES imagery, the use of 30-km-radius, and even moreso of 100-km-radius, circles around a given lightning event inevitably tends to include portions of the image that are not directly pertinent to the electrification/lightning process. In Figure 10, we show the distributions of the *single coldest* cloud pixel within these two radii. These single-coldest-pixel distributions are much narrower than the distributions of Figure 9 and entirely lack the “bridge” feature at $T > -40$ deg C. The centroid of the peak for either non-

NBEs (Figure 10a) or NBEs (Figure 10b) is around -60 deg C. This corresponds to the 13-km height on the radiosonde data (Figure 7). Notice also that the single-coldest-pixel distribution remains significant right out to -70 deg C, corresponding to the nominal tropopause.

The cloud-top-temperature distributions in both Figures 9 and 10 indicate that, as regards affinity for cold cloud tops, NBEs behave roughly as do ordinary lightning events. Both non-NBEs and NBEs are highly selective for being near the coldest cloud tops possible, up to the limit imposed by the tropopause temperature. Both non-NBEs and NBEs are highly unlikely to occur within cloud environments warmer than -40 deg C. This is consistent with observations reviewed elsewhere [Williams, E. R., 2001].

6. METEOROLOGICAL SETTING OF NARROW BIPOLAR EVENTS: COMPARISON WITH MICROWAVE ICE-SCATTERING SIGNATURES

A useful remote-sensing indicator of active cumulonimbus is the scattering of upwelling ~ 37 GHz and ~ 85 -GHz radiation due to large ice hydrometeors (graupel, hail) lofted upward in severe convective cells. This is routinely measured, e.g. aboard TRMM by the TRMM Microwave Imager (TMI) in a wide (760-km) swath aligned within the LIS image [Kummerow, C. et al., 1998]. The TMI is similar to the Special Sensor Microwave Imager (SSM/I) carried by the DMSP satellites. The degree of scattering is greater, the greater the content of graupel and hail high in the cloud. Insofar as this is a similar physical circumstance as necessary for lighting [Baker, M. B. et al., 1999; Blyth, A. M. et al., 2001], the ice scattering and subsequent depression of microwave apparent brightness temperature is expected to correlate with lightning vigor. Focusing on mesoscale convective systems (MCSs), Toracinta and Zipser [2001] compared regional/seasonal climatologies of SSM/I 85-GHz ice-scattering signatures with Optical Transient Detector (OTD) lightning flash rates. They found close positive correlation these two variables’ climatologies in all continental

regions and all seasons, particularly for the most intense MCS clusters.

Boccippio *et al* [2000] have further studied OTD and LIS flash-rate geographical distributions and clarified the land/sea contrast (a factor of ~ 10 in gross flash rate, favoring land) seen by those instruments [see also Figure 1 in Boccippio, D. J., 2002]. They find that the contrast *per storm* is only a factor of ~ 2 , but that marine storms possessing lightning-prone characteristics have wider geographical spacing and less frequent temporal occurrence.

A subsequent study [Toracinta, E. R. et al., 2002] with the TMI, PR, and LIS instruments aboard TRMM addresses the issue of whether all three variables, namely ice-scattering signatures, precipitation-radar cross-sections, and lightning flash rates (respectively) are correlated *for individual storms, not just statistically*. This study shows that the three variables are correlated in individual storms, albeit with some scatter. For example, results on continental tropical South America and Africa regions both show that 40-dBz PR heights are confined to <9 km for storms without LIS lightning, while 40-dBz PR heights extend to <15 km for storms with LIS lightning (see Figure 9 in Toracinta *et al*). Similarly, these same storms show 37-GHz apparent brightness temperatures down only to 250K for storms without LIS lightning, while 37-GHz apparent brightness temperatures extend down to 150K for storms with LIS lightning (see Figure 8 in Toracinta *et al*). The same study verifies the correspondence in reverse also: Continental storms with 37-GHz apparent brightness temperatures below 240K essentially all have LIS-detected lightning, while less than 30% of continental storms with 37-GHz apparent brightness temperatures above 280K have LIS-detected lightning. Similarly, continental storms with PR 30-dBz heights above 11 km essentially all have LIS-detected lightning, while fewer than 30% of continental storms with PR 30-dBz heights below 7 km have LIS-detected lightning (see Figure 10 in Toracinta *et al*).

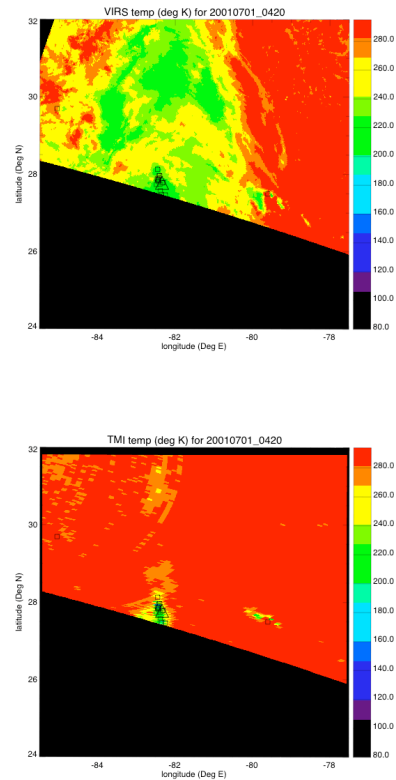


Figure 11: VIRS 10.7-micron brightness temperature (K; top) and TMI 85-GHz PCT (K; bottom) for a single TRMM pass around 04:20 UT on 1 July 2001. The solid black in the lower left is outside the image swath. The image pixel geo-reference assumes an emission altitude of 7 km. Both ordinary (small squares) and NBE (large triangles) events are shown for the crossing time ± 15 minutes.

The previous works have shown a compelling association of the microwave ice-scattering signature with thunderstorm electrification. We now report preliminary results on the relationship between LASA-located lightning events (both ordinary and NBE) and TRMM imagery, both the VIRS 10.7-micron channel and the 85-GHz ice-scattering signature. The present status of this work is that (with the collaboration of Dr. William Boeck) we have selected and archived the TRMM images that cover at least part of the Florida study zone (see Figure 3).

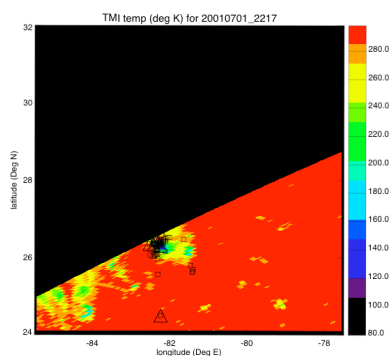
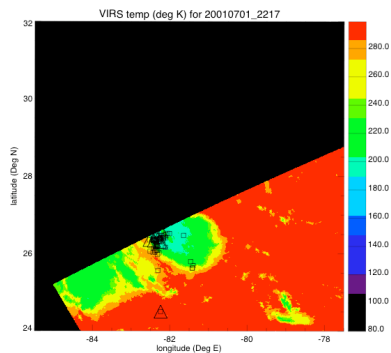


Figure 12: Similar to Figure 11, but for a TRMM pass at 22:17 UT on 1 July 2001. Most of the lightning events are closely associated with ice-scattering signatures. We have not yet determined whether the wayward events far from ice-scattering signatures are poorly geolocated by the LASA array.

Figure 11 shows both VIRS cloud-top temperature (K) and TMI 85-GHz polarization-corrected temperature (PCT; K) for a single TRMM overflight. The TRMM image fields in Figure 11 are each the same size and are centered on the Florida study zone (see Figure 3). The superimposed lightning (black squares and triangles) in Figure 11 are only within the 400-km-radius circle inscribed within the study zone (see Figure 3). The IR image in Figure 11 (top) shows modestly cold cloud tops (~ 220 K, or ~ -50 C) covering much of the image. The lightning is much more localized, however, to a single spot at the lower edge of the swath. The PCT ice-

scattering signature in Figure 11 (bottom) also is much more localized than the cold cloud tops seen by VIRS. Indeed, the lightning and the ice-scattering signature brightness depressions are well correlated (Figure 11 bottom). This is true for both the ordinary (small square symbol) and the NBE (large triangle symbol) lightning events.

Figure 11 and Figures 12 and 13 (all similar to Figure 11, but showing other TRMM passes) imply that the connection of NBEs to ice-scattering signatures is just as pronounced for NBEs as for ordinary lightning.

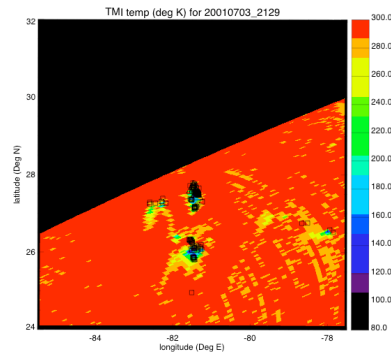
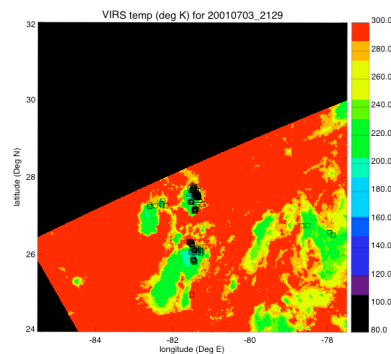


Figure 13: Similar to Figure 11, but for a TRMM pass at 21:29 UT on 3 July 2001.

It should be noted that the dim, arcuate features in the TMI images are artifacts of the constant-nadir-angle, rotating scan format.

REFERENCES

Baker, M. B., A. M. Blyth, H. J. Christian, J. Latham, K. L. Miller, and A. M. Gadian, 1999: Relationship between lightning activity and

- various thundercloud parameters: satellite and modelling studies. *Atmos. Res.*, **51**, 221-236.
- Blyth, A. M., H. J. J. Christian, K. Driscoll, A. M. Gadian, and J. Latham, 2001: Determination of ice precipitation rates and thunderstorm anvil ice contents from satellite observations of lightning. *Atmos. Res.*, **59-60**, 217-229.
- Boccippio, D. J., 2002: Lightning scaling relations revisited. *J. Atmos. Sci.*, **59**, 1086-1104.
- Boccippio, D. J., S. J. Goodman, and S. Heckman, 2000: Regional differences in tropical lightning distributions. *J. Appl. Meteor.*, **39**, 2231-2248.
- Boccippio, D. J., K. Driscoll, W. Koshak, R. Blakeslee, W. Boeck, D. Buechler, H. Christian, and S. Goodman, 2000: The Optical Transient Detector (OTD): Instrument characteristics and cross-sensor validation. *J. Atmos. Oceanic Tech.*, **17**, 441-458.
- Chang, D.-E., J. A. Weinman, C. A. Morales, and W. S. Olson, 2001: The effective of spaceborn microwave and ground-based continuous lightning measurements on forecasts of the 1998 Groundhog Day Storm. *Mon. Weather Rev.*, **129**, 1809-1833.
- Christian, H. J., R. J. Blakeslee, S. J. Goodman, D. A. Mach, M. F. Stewart, D. E. Buechler, W. J. Koshak, J. M. Hall, W. L. Boeck, K. T. Driscoll, and D. J. Boccippio, 1999: The Lightning Imaging Sensor. *11th International Conference on Atmospheric Electricity, Global Hydrology and Climate Center, NASA Marshall Space Flight Center, Huntsville, Alabama, NASA*.
- Holden, D. N., C. P. Munson, and J. C. Devenport, 1995: Satellite observations of transionospheric pulse pairs. *Geophys. Res. Lett.*, **22**, 889-892.
- Jacobson, A. R., 2003: Relationship of intracloud-lightning radiofrequency power to lightning-storm height, as observed by the FORTE satellite. *J. Geophys. Res.*, **108**, 4204, doi:10.1029/2002JD002956.
- , 2003: How do the strongest radio pulses from thunderstorms relate to lightning flashes? *J. Geophys. Res.*, **108**, 4778, doi:10.1029/2003JD003936.
- Jacobson, A. R. and T. E. L. Light, 2003: Bimodal radiofrequency pulse distribution of intracloud-lightning signals recorded by the FORTE satellite. *J. Geophys. Res.*, **108**, 4266, doi:10.1029/2002JD002613.
- Jacobson, A. R., S. O. Knox, R. Franz, and D. C. Enemark, 1999: FORTE observations of lightning radio-frequency signatures: Capabilities and basic results. *Radio Sci.*, **34**, 337-354.
- Jacobson, A. R., K. L. Cummins, M. Carter, P. Klingner, D. Roussel-Dupré, and S. O. Knox, 2000: FORTE radio-frequency observations of lightning strokes detected by the National Lightning Detection Network. *J. Geophys. Res.*, **105**, 15,653.
- Kummerow, C., W. Barnes, T. Kozu, J. Shiue, and J. Simpson, 1998: The Tropical Rainfall Measuring Mission (TRMM) sensor package. *J. Atmos. Oceanic Technol.*, **15**, 809-817.
- Massey, R. S. and D. N. Holden, 1995: Phenomenology of transionospheric pulse pairs. *Radio Sci.*, **30**, 1645-1659.
- Massey, R. S., D. N. Holden, and X.-M. Shao, 1998: Phenomenology of trans-ionospheric pulse pairs: Further observations. *Radio Sci.*, **33**, 1755-1761.
- Petersen, W. A. and S. A. Rutledge, 1998: On the relationship between cloud-to-ground lightning and convective rainfall. *J. Geophys. Res.*, **103**, 14,025-14,040.
- Rison, W., R. J. Thomas, P. R. Krehbiel, T. Hamlin, and J. Harlin, 1999: A GPS-based three-dimensional lightning mapping system: Initial observations in central New Mexico. *Geophys. Res. Lett.*, **26**, 3573-3576.
- Smith, D. A., M. J. Heavner, A. R. Jacobson, X. M. Shao, R. S. Massey, R. J. Sheldon, and K. C. Wiens, 2004: A method for determining intracloud lightning and ionospheric heights from VLF/LF electric field records. *Radio Sci.*, **39**, doi:10.1029/2002RS002790.
- Smith, D. A., K. B. Eack, J. Harlin, M. J. Heavner, A. R. Jacobson, R. S. Massey, X. M. Shao, and K. C. Wiens, 2002: The Los Alamos Sferic Array: A research tool for lightning investigations. *J. Geophys. Res.*, **107**, 10.1029/2001JD000502.
- Smith, D. A., X. M. Shao, D. N. Holden, C. T. Rhodes, M. Brook, P. R. Krehbiel, M. Stanley, W. Rison, and R. J. Thomas, 1999: A distinct class of isolated intracloud lightning discharges and their associated radio emissions. *J. Geophys. Res.*, **104**, 4189-4212.

Suszcynsky, D., A. Jacobson, J. Fitzgerald, C. Rhodes, E. Tech, and D. Roussel-Dupre, 2000: Satellite-based global lightning and severe storm monitoring using VHF receivers. *EOS, Trans. Am. Geophys. Union*, **81**, F91.

Suszcynsky, D. M. and M. J. Heavner, 2003: Narrow Bipolar Events as indicators of thunderstorm convective strength. *Geophys. Res. Lett.*, **30**, 1879, doi:10.1029/2003GL017834.

Thomas, R. J., P. R. Krehbiel, W. Rison, T. Hamlin, J. Harlin, and D. Shown, 2001: Observations of VHF source powers radiated by lightning. *Geophys. Res. Lett.*, **28**, 143-146.

Thomas, R. J., P. R. Krehbiel, W. Rison, T. Hamlin, D. J. Boccippio, S. J. Goodman, and H. J. Christian, 2000: Comparison of ground-based 3-dimensional lightning mapping observations with satellite-based LIS observations in Oklahoma. *Geophys. Res. Lett.*, **27**, 1703-1706.

Toracinta, E. R. and E. Zipser, 2001: Lightning and SSM/I-ice-scattering mesoscale convective systems in the global tropics. *J. Appl. Meteor.*, **40**, 983-1002.

Toracinta, E. R., D. J. Cecil, E. J. Zipser, and S. W. Nesbitt, 2002: Radar, passive microwave, and lightning characteristics of precipitating systems in the tropics. *Mon. Wea. Rev.*, **130**, 802-824.

Wescott, E. M., D. D. Sentman, M. J. Heavner, D. L. Hampton, and O. H. Vaughan, Jr., 1998: Preliminary results from the Sprites94 aircraft campaign: Blue Jets. *Geophys. Res. Lett.*, **22**, 1209-1212.

Williams, E. R., 2001: Chapter 13: The Electrification of Severe Storms. *Severe Convective Storms*, C. A. I. Doswell, Ed., American Meteorological Society.

Williams, E. R., M. E. Weber, and R. E. Orville, 1989: The relationship between lightning type and the convective state of thunderstorms. *J. Geophys. Res.*, **94**, 13213-13220.

Zipser, E. J., 1994: Deep cumulonimbus cloud systems in the tropics with and without lightning. *Mon. Weather Rev.*, **122**, 1837-1851.

Zipser, E. J. and K. R. Lutz, 1994: The vertical profile of radar reflectivity of convective cells: A strong indicator of storm intensity and lightning probability? *Mon. Weath. Rev.*, **122**, 1751-1759.